Received: 18 June 2019 | Revised: 17 October 2019 | Accepted: 12 November 2019

DOI: 10.1002/jsp2.1074

JOR Spine OPEN ACCESS

RESEARCH ARTICLE

Morphological and biomechanical effects of annulus fibrosus injury and repair in an ovine cervical model

Rose G. Long[1] | Stephen J. Ferguson[2] | Lorin M. Benneker[3] | Daisuke Sakai[4] | Zhen Li[5] | Abhay Pandit[6] | Dirk W. Grijpma[7] | David Eglin[5] | Stephan Zeiter[5] | Tanja Schmid[5] | Ursula Eberli[5] | Dirk Nehrbass[5] | Theodor Di Pauli von Treuheim[8] | Mauro Alini[5] | James C. Iatridis[8] | Sibylle Grad[5]

[1]Department of Genetics, Harvard Medical School, Boston, Massachusetts

[2]ETH Zurich, Institute for Biomechanics, Zurich, Switzerland

[3]Department for Orthopaedic Surgery, Spine Unit, Inselspital, University Hospital of Bern, Bern, Switzerland

[4]Department of Orthopaedic Surgery, Tokai University School of Medicine, Kanagawa, Japan

[5]AO Research Institute Davos, Davos Platz, Switzerland

[6]CÚRAM, Center for Research in Medical Devices, National University of Ireland, Galway, Ireland

[7]University of Twente, Technical Medical Centre, Department of Biomaterials Science and Technology, Faculty of Science and Technology, Enschede, The Netherlands

[8]Leni & Peter W. May Department of Orthopaedics, Icahn School of Medicine at Mount Sinai, New York, New York

Correspondence
James C. Iatridis, Leni & Peter W. May Department of Orthopaedics, Icahn School of Medicine at Mount Sinai, 1 Gustave Levy Place, Box 1188, New York, NY 10029-6574.
Email: james.iatridis@mssm.edu

Sibylle Grad, AO Research Institute Davos, Clavadelerstrasse 8, 7270, Davos Platz, Switzerland.
Email: sibylle.grad@aofoundation.org

Funding information
AO Foundation; AOSpine; National Institute of Arthritis and Musculoskeletal and Skin Diseases, Grant/Award Number: R01AR057397; Whitaker International Fellows and Scholars Program

Abstract

Tissue engineering repair of annulus fibrosus (AF) defects has the potential to prevent disability and pain from intervertebral disc (IVD) herniation and its progression to degeneration. Clinical translation of AF repair methods requires assessment in long-term large animal models. An ovine AF injury model was developed using cervical spinal levels and a biopsy-type AF defect to assess composite tissue engineering repair in 1-month and 12-month studies. The repair used a fibrin hydrogel crosslinked with genipin (FibGen) to seal defects, poly(trimethylene carbonate) (PTMC) scaffolds to replace lost AF tissue, and polyurethane membranes to prevent herniation. In the 1-month study, PTMC scaffolds sealed with FibGen herniated with polyurethane membranes. When applied alone, FibGen integrated with the surrounding AF tissue without herniation, showing promise for long-term studies. The 12-month long-term study used only FibGen which showed fibrous healing, biomaterial resorption and no obvious hydrogel-related complications. However, the 2 mm biopsy punch injury condition also exhibited fibrotic healing at 12 months. Both untreated and FibGen treated groups showed equivalency with no detectable differences in histological grades of proteoglycans, cellular morphology, IVD structure and blood vessel formation, biomechanical properties including torque range and axial range of motion,

Pfirrmann grade, IVD height, and quantitative scores of vertebral body changes from clinical computed tomography. The biopsy-type injury caused endplate defects with a high prevalence of osteophytes in all groups and no nucleus herniation, indicating that the biopsy-type injury requires further refinement, such as reduction to a slit-type defect that could penetrate the full depth of the AF without damaging the endplate. Results demonstrate translational feasibility of FibGen for AF repair to seal AF defects, although future study with a more refined injury model is required to validate the efficacy of FibGen before translation.

KEYWORDS

annulus fibrosus, intervertebral disc, intervertebral disc herniation, ovine in vivo model, tissue engineering

1 | INTRODUCTION

Defects of the intervertebral disc (IVD), which include injuries to the annulus fibrosus (AF) and herniation, are highly associated with disabling back and neck pain.[1,2] Extrusion of nucleus pulposus or AF tissue as an IVD herniation is a known and specific cause of pain and disability.[3] Surgery can relieve disability from the neuropathy but does not repair the AF. The urgent clinical need for AF repair stems from the risk of reherniation following discectomy surgery, with reherniation rate as high as 27% for defects larger than 6 mm, and an average rate of 15%.[4] Unrepaired AF defects can also lead to progression of IVD degeneration as an additional source of pain and disability. Developing AF repair strategies is therefore a research priority, and the use of large animal models of AF injury and repair is necessary to accelerate translation of AF repair strategies. The present work describes progress toward establishing and translating AF repair models using a short-term (1-month) and long term (12-month) ovine model of AF injury.

Ovine IVDs are a popular IVD pathology model[5–9] due to their size, and the biochemical, cellular, and mechanical environment. Lumbar ovine IVDs are approximately 1/3 the size of human IVDs,[10] and capture the diffusion limited nutrient and oxygen transport environment observed in human IVDs.[11,12] As in human,[13] ovine nucleus pulposus cells do not express a notochordal phenotype during skeletal maturity.[14] Intradiscal pressures up to 3.5 MPa have been observed in the lumbar IVDs of sheep,[15] suggesting the model provides rigorous mechanical loading. Ovine lumbar and cervical spine levels have been used because of their biomechanical similarities with human IVDs, and the larger IVD height of sheep cervical spine levels makes them an attractive model for evaluating spinal implants.[16]

Annular closure devices include sutures, such as the unavailable Xclose Tissue Repair System (Anulex Technologies, Minnetonka, Minnesota) and the similar but available AnchorKnot, (Anchor Orthopedics, Mississauga, Ontario, Canada),[17] and a mesh barrier which anchors to the vertebral body called Barricaid (Intrinsic Therapeutics, Woburn, Massachusetts). The Barricaid is under current clinical investigation with promising results including decreased disability, increased IVD height and reduced rate of recurrent IVD herniation, but had a higher frequency of endplate complications at 2[18]) and 3 years.[19] In addition to mechanical repairs, there are a range of AF replacement materials including electrospun poly-e-caprolactone[20,21] and hyaluronic acid with polyethylene[22] (material properties reviewed in Reference 23). Void filling biomaterials which can be injected with or without cells, such as collagen,[24] were recently reviewed in Reference 25. While many biomaterials exist for AF repair, those with regulatory approval can be further improved, and those that are not approved need further validation. Due to the high clinical need, AF repair remains an active area of research (reviewed in[26,27]), and this study uses a preclinical large animal model to evaluate multiple biomaterial repair strategies for AF repair. Fibrin crosslinked with genipin (FibGen) is an adhesive hydrogel optimized for AF repair by tuning its formulation to match the shear modulus of human AF.[28] Previous in vitro studies reported a reduction of IVD height loss in a bovine AF defect organ culture model[29] and low herniation risk in ex vivo mechanical testing of the bovine IVD.[30] A polytrimethylene carbonate (PTMC) based porous scaffold showed the ability to immediately restore the IVD height after implantation in an AF defect of a bovine loaded organ culture model,[31] and offers potential for delivery of bioactive factors and cells. A polyurethane (PU) membrane sutured onto the AF was used to prevent herniation of this PTMC scaffold, which remained in place within the AF defect for 2 weeks in an organ culture bioreactor system under mechanical load.[31] The success of FibGen adhesive, PTMC scaffold, and the PU membrane in prior ex vivo testing motivate their in vivo use in a large animal model as an important next step in translation for an AF repair strategy.

The purposes of this in vivo study were (a) to perform a 1-month screening study to evaluate the feasibility of FibGen, PU membrane, and PTMC as a composite strategy for AF repair in vivo; and (b) to perform a 12-month long-term study of biopsy punch AF injury and to evaluate the performance of FibGen. The 1-month screening study compared the histological appearance of injured cervical IVDs treated with three different composite repair strategies: injectable FibGen

only, FibGen with membrane, and FibGen with scaffold and membrane. The long-term study compared histological appearance, degeneration using Pfirrmann grade, IVD height, vertebral body changes using computed tomography (CT), and biomechanical behavior of untreated and FibGen treated injured cervical IVDs.

2 | MATERIALS AND METHODS

2.1 | Animals and pre-op care

The studies were approved by the relevant Swiss authorities (Cantonal authorities in Graubünden, Switzerland; Permission # 40/2014). Four skeletally mature female Swiss White Alpine sheep (age range: 2-4 years old, weight range 51.5-63 kg) were enrolled in the screening study; while 10 sheep (age range: 3-5 years old, weight range 74-89 kg) were enrolled in the long-term study. Prior to the start of the study, the animals were acclimatized for 2 weeks at the Association for Assessment and Accreditation of Laboratory Animal Care International (AAALAC) approved facility. During this time, they were group housed under a 12 hours dark/ light cycle and fed with hay, mineral lick, and hand-fed grain to gain familiarity with caregivers. Before the surgery, the sheep were assessed to be in good health based on a complete physical clinical assessment by a veterinarian.

2.2 | Preclinical model overview

2.2.1 | Screening study

In each sheep (four animals), a 2 mm annular defect was created with a biopsy punch in four cervical levels: C2-C3, C3-C4, C4-C5, and C5-C6. IVDs in the Injured group were not repaired (n = 4). The biopsy punch injury was used because it is repeatable, clinically relevant and has precedent in the literature.[31,32] IVDs in the treatment groups were repaired by either injection of FibGen (n = 4), injection of FibGen and suture of PU membrane onto the defect (n = 4), or implantation of PTMC scaffold with sealing by FibGen and suturing of PU membrane (n = 4) (Figure 1G). Treatments were rotated systematically by level (C2-C5) to avoid potential level bias. *Long-term study*: In each sheep (10 animals), a 2 mm annular injury was created with a biopsy punch in three cervical levels: C2-C3, C3-C4, and C4-C5. IVDs at levels C5-C6 and C6-C7 were used as intact controls (termed Intact group, n = 20). In each sheep, one cervical IVD (from C2-C5) which had an annular defect was not repaired (termed Injured group, n = 10). Immediately after annular injury creation, two cervical IVDs (from C2-C5) were repaired with an injection of FibGen (termed FibGen group, n = 20) (Figure 1H). Assignment to Injured or FibGen groups was rotated systematically by level to avoid potential level bias such that Injured group had 3 C2-C3, 4 C3-C4, and 3 C4-C5 and the FibGen group had 7 C2-C3, 6 C3-C4, and 7 C4-C5.

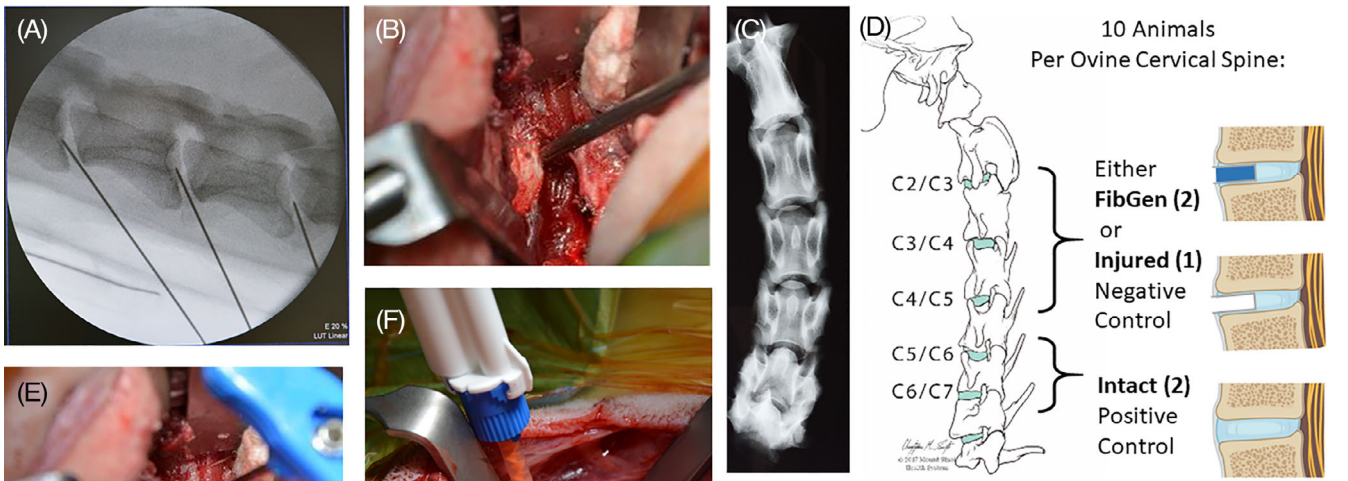

Condition	Histology
Injured	4
FibGen	4
FibGen and membrane	4
FibGen, membrane and scaffold	4

Condition	Biomechanics & µCT	Clinical CT & MRI	Histology
FibGen	10	20	10
Injured	5	10	5
Intact	0	20	10

FIGURE 1 Surgical approach and study design of the long-term study. A, Surgical approach was guided radiographically using a C-arm. B, The intervertebral disc was exposed with an anterolateral approach. C, Radiograph of C2-C7 demonstrating convexity of the inferior endplate. D, The three cervical (C2-C5) IVDs of 10 animals were injured with a biopsy punch and two were repaired with FibGen. E, The exposed intervertebral IVD was injured with a 2 mm diameter biopsy punch. F, The FibGen repair was delivered with a mixing tip syringe. G, All Injured untreated (n = 10) and FibGen repaired levels (n = 20) from 10 animals were subjected to computed tomography and magnetic resonance imaging and were evenly distributed to histological or biomechanical analysis

2.3 | Surgical intervention

After sedation with Detomidine (0.04 mg/kg intramuscular [IM], Domosedan, Pfizer AG) in the stable, anesthesia was induced using intravenous Midazolam (0.2 mg/kg IV, Midazolam Sintetica, Sintetica SA) and Ketamine (4 mg/ kg IV, Ketasol-100, Graeub AG). Animals were intubated, and anesthesia was maintained with isoflurane-oxygen (1.5-1.8% V/V in 0.6-1 L/min oxygen, Isofluran, Baxter, Baxter AG). Preoperative analgesia consisted of Carprofen (1.4 mg/kg IV, Rimadyl Rind, Pfizer AG) and intraoperatively Fentanyl (5 μg/kg/h IV, Sintenyl, Sintetica) was infused. For antibiotic prophylaxis Ceftiofur (2.2 mg/kg, Excenel, Zoetis) was given perioperatively and every 24 hours for 5 days post op.

For the surgery, the sheep were placed in dorsal recumbency and, under aseptic technique, the cervical levels were exposed through a ventral approach from the right side.[32] A longitudinal incision and blunt preparation between the sternocleidoideus and longus colli muscles/carotid sheath (lateral) and the trachea (medial) exposed the anterior aspect of the IVD (C2/3-C6/C7). After confirmation of the correct level with the C-arm X-ray (Figure 1A), IVDs from C2-C5 (C2-C6 for the screening study) (Figure 1C,D) were then subjected to an anterolateral 2 mm diameter biopsy punch injury approximately 4 mm deep (Figure 1B,E). The wound was closed in three layers (fascia, subcutaneous and intracutaneous suture, all Monocryl 3-0 [Ethicon, Somerville, New Jersey]) and was covered with a spray bandage and a stent (rolled cotton swabs, fixation with Ethilon 2-0 [Ethicon, Somerville, New Jersey]).

Postoperative analgesia consisted of Buprenorphine (0.05 mg/kg IM every 8 hour for 3 days), Carprofen (1.4 mg/kg SC every third days for 5 days, Rimadyl Rind Pfizer AG) as well as Fentanyl (2 μg/kg/h for 72 hours, Durogesic Matrix patches, cutaneous). Animals were housed in groups of two sheep first and then in larger groups of up to five sheep under the same conditions as listed above. Animal welfare was assessed using a score sheet twice daily for 3 days, daily for four additional days, and then once weekly.

2.4 | AF repair

FibGen was prepared freshly prior to surgery by dissolving fibrinogen (Sigma-Aldrich) in filtered (12 μm) Phosphate Buffered Saline (PBS) at 140 mg/mL. The mixture was exposed to ultraviolet light for 1 hour. Thrombin (40 μL of 1000 U/mL) (Sigma-Aldrich, Buchs, Switzerland) was added to 226.8 μL of PBS. Genipin (Wako Chemicals USA Inc., Richmond, Virginia) dissolved in dimethyl sulfoxide (20.25 μL of 6 mg/mL) was added to the thrombin/PBS. The fibrinogen (0.8 vol. fraction) and thrombin/PBS/genipin (0.2 vol. fraction) were concomitantly injected with a 4:1 dual barrel syringe (Pearson Dental, Sylmar, California) to completely fill the annular defect (Figure 1F). *Screening Study*: PTMC scaffolds and PU films used for the screening study were prepared as described elsewhere.[31] For the FibGen repair (n = 4), FibGen was injected as described above. For the FibGen + membrane repair (n = 4), FibGen was injected into the defect which was sealed by suturing a PU film onto the surrounding AF tissue (4-point suture) using a 4-0 Prolene (Ethicon, Somerville, New Jersey). For the FibGen + membrane + scaffold repair (n = 4), a conical PTMC scaffold of 2 mm (outer side) and 3 mm (inner side) in diameter and 4 mm length was press-fit into the AF defect and filled with FibGen hydrogel. The defect was then covered with a PU film sutured onto the surrounding AF tissue as outlined above.

2.5 | In vivo clinical CT

In the long-term study, in vivo computed tomography (CT) scans of the cervical IVDs (C2-C7) were acquired at a resolution of 0.63 mm using 130 kV potential, an exposure of 180 mAs and a slice thickness of 1 mm (SOMATOM Emotion 6, Siemens, Germany) right after surgery and consecutively every 3 months until 12 months. The scans were performed under general anesthesia using the same protocol as above. Each cervical IVD was scored from 0 to 4 based on bone formation by a blinded veterinarian. A score of 0 indicated normal appearance of vertebral bones, 1 indicated slight roughening, 2 indicated small osteophyte, 3 indicated larger osteophyte, and 4 indicated large new bone formation bridging the IVD space (Figure S1).

2.6 | Euthanasia and sample harvest

The animals of the screening study were euthanized after 1 month, while the animals of the long-term study were euthanized after 12 months by an overdose of pentobarbital (7.5 g IV, Esconarkon), and the cervical spine was harvested. Musculature and posterior elements were removed and vertebrae (C2-C7) were bisected transversely using a butcher saw. *Screening Study*: Injured IVDs treated with FibGen (n = 4), FibGen and PU (n = 4), PTMC with FibGen and PU (n = 4), and untreated injured IVDs (n = 4) were fixed in ethanol and processed for histology. *Long-term Study*: For biomechanical analyses, Injured (n = 5) and FibGen (n = 10) repaired motion segments were isolated with a transverse cut through the adjacent vertebra, relieved of posterior elements including facet joints, sealed in plastic, wrapped in saline soaked tissue paper, and frozen at −20°C. For histological analyses, Injured (n = 5), Intact (n = 10) and FibGen (n = 10) repaired IVDs were fixed in ethanol (Figure 1G).

2.7 | MRI

MRI was acquired directly after harvesting with a 1.5 T MRI scanner (Philips Medical Systems, Intera), using a sense-body imaging coil with sagittal projections and T2-weighted (TR = 2000, TE = i*20 ms, i = 1, 2…8) sequences with a 320 × 320 mm field of view, 8 mm slice thickness, 8.8 mm slice spacing. Three blinded board-certified orthopedic surgeons assessed the Pfirrmann grade of each cervical IVD. Disc and vertebral body height was measured by tracing a spline along the cartilaginous endplate with FIJI[33] and calculating the Euclidean distance between the dorsal, central and ventral parts of the spline with a

TABLE 1 Biomechanical parameters for Injured and FibGen samples including axial compliance and tensile stiffness. Data are presented as mean ± SD

Parameter	Injured	FibGen	*P* value
Axial compressive compliance (μm/N)	1.22 ± 0.15	1.18 ± 0.14	.47
Axial tensile compliance (μm/N)	5.34 ± 1.21	4.80 ± 0.80	.49
2° tensile stiffness (Nmm/°)	535 ± 392	565 ± 199	.44
4° tensile stiffness (Nmm/°)	1055 ± 578	1217 ± 288	.67

custom Matlab script. Central disc height is presented. Disc height index was calculated by normalizing the sum of the IVD heights with the sum of the inferior vertebral body heights.[34]

2.8 | Biomechanical testing

Motion segments were thawed overnight at 4°C after which the vertebral bodies were embedded in polymethylmethacrylate (Suter

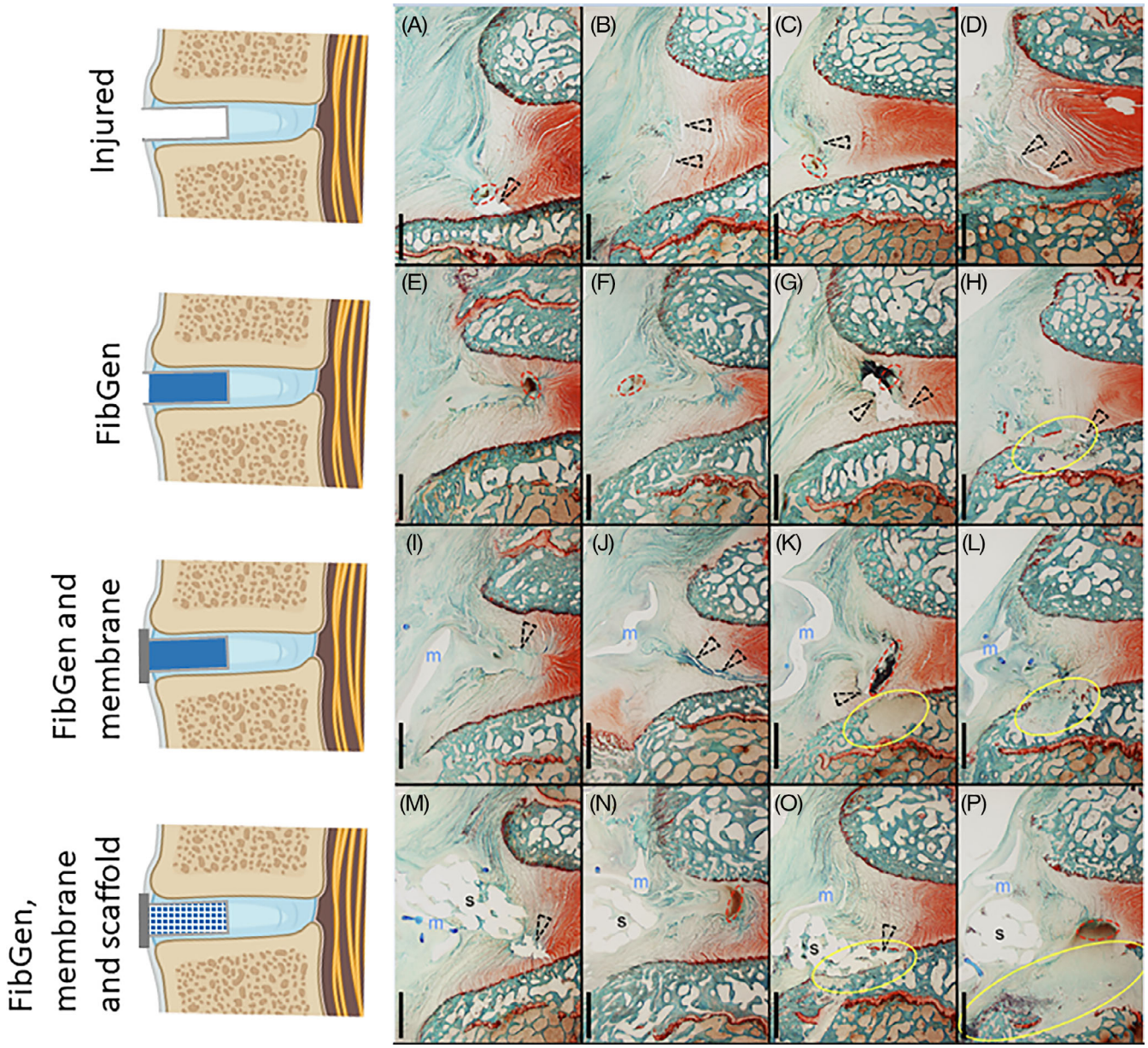

FIGURE 2 Histological findings 1 month after surgery in screening study. A-D, Untreated annulus fibrosus (AF) defects (Injured group) demonstrated discontinuous tissue (clefts, black arrow) and blood vessels (red circle); E-H, FibGen treated IVDs demonstrated discontinuous tissue, (clefts, black arrow), blood vessels (red circle), and endplate damage (yellow circle); I-L, FibGen with membrane repair showed displaced membrane (m), discontinuous tissue (black arrow), blood vessels (red circle) and endplate damage (yellow circle). M-P, FibGen with membrane and scaffold had discontinuous tissue (black arrow), displaced scaffold (s) and membrane (m). Overview microphotographs of thick-sections of sheep cervical intervertebral IVDs (nondecalcified, resin-embedded, Safranin O-Fast Green-stained material; scale bar: 2 mm; image orientation: left = ventral, bottom = caudal)

Kunstoffe AG, Fraubrunnen, Switzerland) and fixed to the servo hydraulic system (MiniBionix II 858, MTS Systems Corp., Eden Prairie, Minnesota) using custom holders and an X-Y table to eliminate shear forces. Each specimen was subjected to cyclic sinusoidal axial loading between 100 N to −250 N at three frequencies: 0.1, 1, and 2 Hz. The compressive load corresponded to intradiscal pressure of 1.1 MPa in Merino sheep.[15] Then, each specimen was subjected to torsional loading at two rotations: first ±2°, then ±4° at three frequencies: 0.1, 1, and 2 Hz. The rotation was informed by the limits of human physiological motion which are ±4°.[36] The number of cycles were: 20 cycles for 0.1 Hz, 30 cycles for 1 Hz, and 100 cycles for 2 Hz. However, at 1 and 2 Hz, the mechanical test system did not adequately control to the target tensile loads of 100 N or target compressive loads of 250 N, so only 0.1 Hz loading was analyzed. Parameters were measured on the 20th cycle of the 0.1 Hz loading. Machine data of axial load, axial displacement, torque and torsional angle were continuously recorded at 128 Hz. Intact biomechanical data from C2 to C5 were taken from previously published data acquired using the same test protocol and same age and type of sheep.[32]

The torque range was calculated as the total torque developed between ±2° and ± 4°. The axial range of motion was calculated as the total displacement between the common maximum and minimum loads, 97 N and −224 N, respectively. The torsional stiffness was calculated as the slope of the linear fit of the maximal 20% of the torque-rotation curve. The axial compliance was calculated as the slope of the maximal 20% of the axial force-displacement curve. The neutral zone length and stiffness were calculated as the average of both loading directions using the double sigmoid model.[36]

2.9 | Histological analysis

Motion segments were fixed in 70% ethanol and embedded in methyl-methacrylate. Mid-sagittal sections (300 µm wide) were stained with Safranin O/Fast Green. *Long-term Study*: Safranin O/Fast Green stained sections from FibGen and Injured intervertebral IVDs were graded by three observers using a six category grading scheme adapted from Shu et al. (Table 1).[38] The categories were (a) proteoglycan depletion; (b) IVD structure/lesion morphology; (c) cellular morphology; (d) blood vessel ingrowth; (e) cell influx into lesion; and (f) cleft formation. The sum score was calculated by summing grades across categories. All sections were graded by three blinded

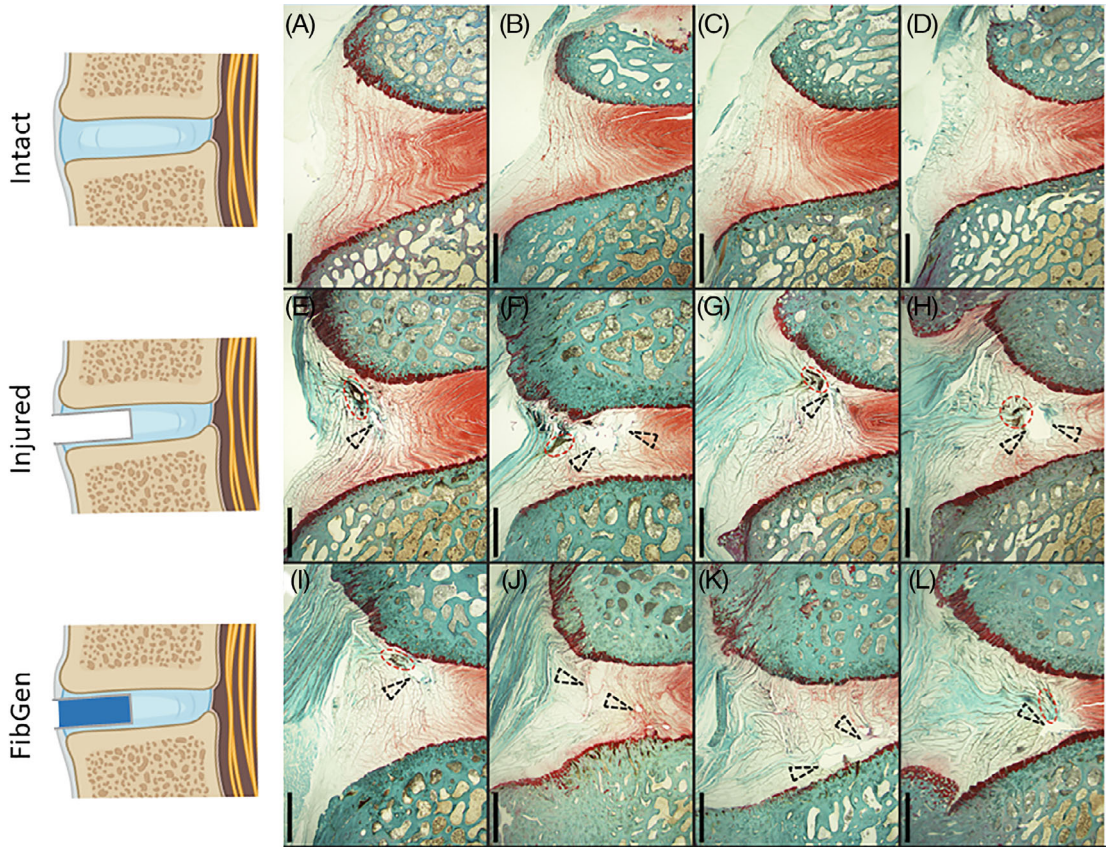

FIGURE 3 Histological findings 12 months after surgery in long-term study. A-D, Intact samples showed highly aligned AF lamellae. E-H, Injured specimens had discontinuous AF tissue (arrow), blood vessels (red circle), and endplate disruption. I-L, FibGen repaired specimens showed discontinuous AF tissue (arrow), blood vessels and endplate disruption. Overview microphotographs of thick-sections of sheep cervical intervertebral IVDs (nondecalcified, resin-embedded, Safranin O-Fast Green-stained material; scale bar: 2 mm; image orientation: left = ventral, bottom = caudal)

observers. Biopsy tissue was collected and underwent von Kossa staining for mineralization.

2.10 | Statistical analysis

Differences between FibGen and Injured biomechanical response were assessed with nonparametric T test using Prism version 7 for Windows (GraphPad Software, La Jolla, California). Differences in Pfirrmann grade and histology grades were assessed with nonparametric two-way ANOVA for grader and treatment, differences in clinical CT score were assessed with two-way nonparametric ANOVA for treatment and time, differences in disc height index and disc height was assessed with nonparametric one way ANOVA for treatment, all with nonparametric post hoc treatment comparisons, using R for Windows (The R Foundation for Statistical Computing,[39]). In box plots, whiskers represent 1.5* interquartile range and the hinges span the first and third quartiles whereas in scatter plots, bars represent the median and interquartile range. Statistically important difference was identified with $P < .05$. We calculated the average measures intraclass coefficient to measure interjudge reliability for the histology scores using a two way mixed model which is for random samples and fixed judges. Here, the intraclass coefficient is reliability of the average of these three judge's rating, with 1 indicated high agreement and 0 indicating no agreement.[40]

3 | RESULTS

3.1 | Animals

All animals recovered well from the surgical intervention. However, in the screening study, two animals had wound dehiscence which healed uneventfully after treatment (wound care with debridement). These animals and one animal that developed a seroma were treated with prolonged antibiotic coverage extending two additional weeks. In the long-term (12 months) study, no complications occurred. One animal continuously lost weight over the duration of the study and a chronic parasitic infestation (liver flukes) was identified post mortem. No abnormal clinical behavior was observed during the entire duration of the study in all animals.

3.2 | Histological analysis

3.2.1 | Screening study

The outcome of the 1-month screening study was assessed qualitatively by light microscopy using Safranin-O/Fast Green stained sections (Figure 2). In untreated AF defects, clefts of different dimensions and orientations were observed adjacent to the lesion site; furthermore, brownish stained blood vessels were found in most samples

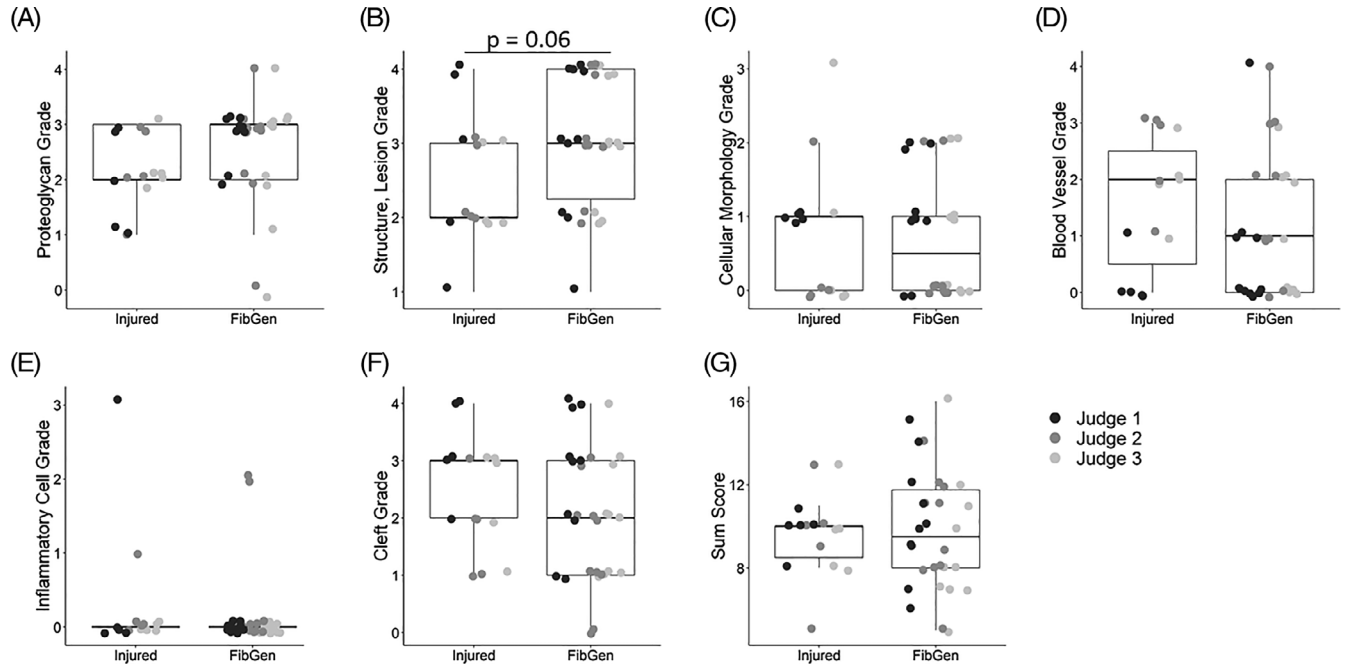

FIGURE 4 Semiquantified histological findings after 12 months. A, No difference in proteoglycan grade, defined by Safranin O-Fast Green staining intensity, was detected between Injured and FibGen groups. B, A trend of difference in the structure grade, defined by propagation of lesion into NP, was detected between Injured and FibGen groups ($P = .06$). C, No difference in the cellular morphology, defined by presence of rounded chondrocytes, was detected between Injured and FibGen groups. D, No difference in blood vessel ingrowth was detected between Injured and FibGen groups. E, No difference in cleft grade, defined by radial cleft area, was detected between Injured and FibGen groups. F, No difference in cleft grade, defined by radial cleft area, was detected between Injured and FibGen groups. G, No difference in sum score was detected between Injured and FibGen groups. For all categories, a grade of 0 indicated no changes while a grade of 4 indicated most severe changes

with AF defects (Figure 2A-D). In FibGen treated defects, large clefts were noted in 1/4 cases, while presence of vessels was also identified similar to the untreated defects (Figure 2E-H). Sealing of the FibGen treated defect with a PU film sutured onto the AF tissue did not influence the histological outcome; in fact, there were signs of displacement of the PU membrane in most cases (Figure 2I-L). Similarly, the PTMC scaffold did not remain stable in the defect but was dislocated in most cases (Figure 2M-P). In all treatment groups, discontinuation of the endplate was evident. This damage was observed in 1-2 cases/group and was mainly located on the caudal endplate. *Long-term study*: The outcome of the main (12-month) study was assessed semiquantitatively using Safranin-O/Fast Green stained sections (Figure 3). The Intact group demonstrated highly aligned AF lamella, and intense Safranin-O staining in the NP and inner AF. The cancellous bone had uniform trabeculae distally. The Injured (Figure 3E-H) and FibGen (Figure 3I-L) groups showed increased trabecular bone density and an uneven endplate surface, suggesting bone remodeling. The Injured (Figure 3E-H) and FibGen (Figure 3I-L) groups also had discontinuous AF tissue and brownish staining which may be indicative of intradiscal blood vessels. The frequency of positive von Kossa stain indicating mineralization in tissue removed during injury creation was 3/10 (30%) for Injury group and 4/20 (20%) for the FibGen group.

Sagittal sections from FibGen (n = 10 from 10 animals) and Injured (n = 5 from 5 animals) groups were graded for (a) proteoglycan depletion; (b) IVD structure/lesion morphology; (c) cellular morphology; (d) blood vessel ingrowth; (e) cell influx into lesion; and (f) cleft formation (Figure 4, Table S1). No differences were detected between the Injured and FibGen treated groups for any category (Figure 4A-E) nor the sum score (Figure 4F), although FibGen had a statistical trend of higher structure/lesion grade ($P = .06$) (Figure 4B). Few FibGen and Injured IVDs had cellular influx and new blood vessel formation in response to the biopsy punch injury (Figure 5), with positive histology scores for 2/5 Injured and 2/10 FibGen IVDs (Figure 4E). The intraclass coefficients for each category were: (a) proteoglycan depletion, 0.78; (b) IVD structure/lesion morphology, 0.79; (c) cellular morphology, 0.68; (d) blood vessel ingrowth, 0.68; (e) cell influx into lesion, 2e-7; and (f) cleft formation, 0.20.

3.3 | In vivo clinical CT imaging

The Injured and FibGen groups showed an increase in clinical CT score compared to 0-month baseline (Figure 6A). All samples had a score of 0 at 0 months, indicating no bone formation (Figure 6B). For the FibGen group, the score was significantly higher at 3 months ($P = .01$), 6 months ($P = .005$), 9 months ($P = 3.1 \times 10^{-5}$) and 12 months ($P = 5.8 \times 10^{-5}$). In the Injured group, the score was significantly higher at 9 months ($P = .02$) and 12 months ($P = .01$), with a trend of significance at 6 months ($P = .07$). When comparing between groups at each timepoint, the Intact group had lower score at 3, 6, 9, and 12 months, compared to the Injured ($P = .006$, 5.4×10^{-5}, 5.4×10^{-5}, 0.00019) and FibGen groups ($P = .0003$, 5.4×10^{-5}, 5.4×10^{-5}, 6.7×10^{-5}). 3D reconstructions from biomechanics specimens, which underwent microtomography in addition to the clinical CT, demonstrate increased bone formation with increased clinical CT score (Figure S1).

3.4 | MRI

The Pfirrmann grade of the Injured ($P < .001$) and FibGen ($P < .001$,) groups were lower than the Intact samples, and no difference was detected between Injured and FibGen specimens ($P = .46$) (Figure 7A, D). The IVD height of Intact group was less than that of Injured ($P < .002$) and FibGen ($P < .001$) groups (Figure 7B). The disc height index, which is disc height normalized by the inferior vertebral body height, was higher for Intact samples compared to FibGen ($P < .002$) and Injured ($P < .002$) (Figure 7C).

3.5 | Biomechanical analysis

No differences were detected for torsional or axial biomechanical behavior of FibGen and Injured IVDs, as seen in representative torque-rotation and force-displacement curves from Injured (level C2-C3) and FibGen (level C3-C4) treated IVDs (Figure 8A,F). Previous results suggest intact IVDs from C2 to C3 and C3 to C4 have comparable mechanical behavior.[32] There were no detected differences in torque range (Figure 8B,D), neutral zone length (Figure 8C,E), axial range of motion (Figure 8G), axial neutral zone length (Figure 8H), torsion stiffness nor axial compliance (Table 1).

4 | DISCUSSION

This study applied an ovine cervical IVD biopsy injury model to evaluate the in vivo response of multiple AF repair methods. An 1-month screening study evaluated multiple composite AF repair strategies for their herniation risk using histological evaluation as output. The long-term 12-month study evaluated effects of AF injury and FibGen repair on IVD and vertebral body structure and function using CT, MRI, histology, and biomechanical assessments.

The 1-month screening determined the applicability and the persistence of FibGen gel and PTMC scaffold within the AF defect since these biomaterials had previously been shown to have beneficial effects in an organ culture model of AF injury.[31] This current study showed dislocations of both the PTMC scaffold and the supporting PU membrane 1 month after surgery. This finding may be attributed to the more rigorous mechanical environment in the cervical IVD in vivo[15] compared to the merely axial simulated-physiological load that was applied in prior organ culture studies on isolated bovine IVDs.[31] FibGen repair had no negative effects at 1 month and the PU membrane was not necessary to prevent herniation. Consequently, the subsequent long-term study focused on the application of FibGen for repair of the AF defect.

FibGen repair was delivered into the defect via injection, and the effects of IVD repair were compared to unrepaired injured and intact IVDs. Results demonstrated equivalency between FibGen and Injured groups. No significant changes in biomechanical response were observed between Injured and FibGen groups. Histologically, altered AF fiber morphology and intradiscal vessel formation were observed in the Injured and FibGen groups. Together, these results suggest fibrotic healing was occurring within 12 months of the injury in Injured and FibGen groups. While the biopsy defect resulted in disruption to AF morphology and vertebral bodies that remained at 12-months, the degeneration was relatively mild with no signs of nucleus pulposus herniation or marked IVD height loss. Relatively high variance in the biomechanical data could be attributed to vertebral body morphology changes and osteophyte formation. A repeated measures study design found a 5 to 10% reduction in axial range of motion and torque range from an identical injury on ovine cervical

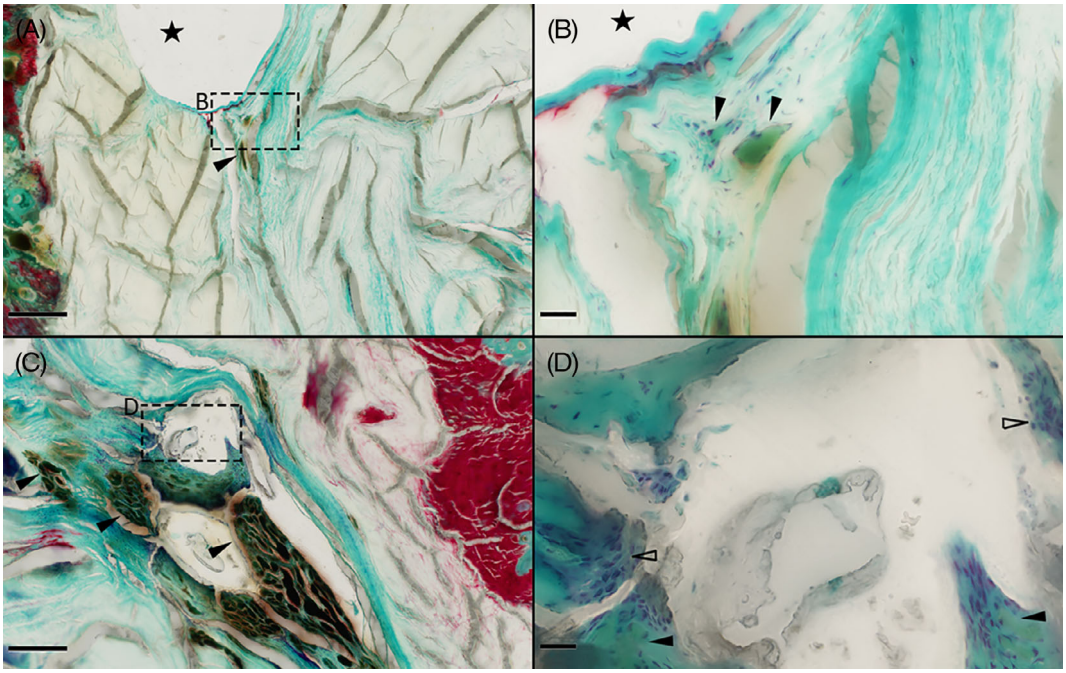

FIGURE 5 Cellular influx and response to injury. A, Injured IVD with endplate on right (stained red) demonstrates cleft formation (star), greenish-stained collagen fiber formation (fibrosis), and low-grade blood vessel ingrowth (neovascularization, black arrowhead) along the defect canal. B, Cells are present at blood vessels (black arrowhead) adjacent to defect (star). C, FibGen IVD had blood vessel ingrowth (black arrow heads). D, Rounded cells are present (empty arrowheads) near blood vessels (black arrowheads). Ethanol-fixed, nondecalcified, resin-embedded, SafraninO/Fast Green-stained thick-sections, scale bar A + C: 200 μm; B + D: 20 μm

(A)

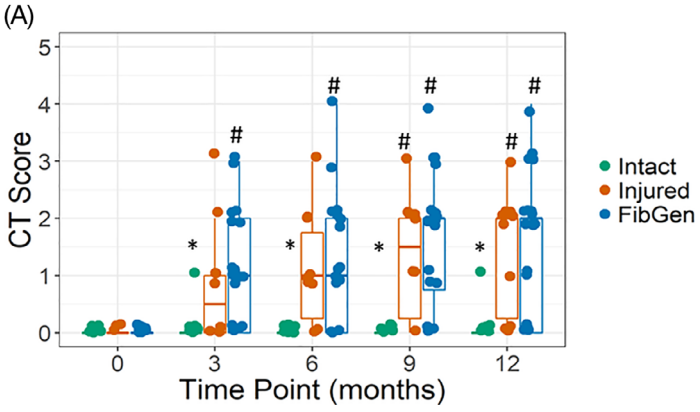

(B)

CT Score	Description
0	Normal appearance of vertebral bones
1	Less distinct bone margins in endplate areas, slight roughening
2	Small osteophyte
3	Larger osteophyte, expanding towards next vertebral body or starting to bridge disc space
4	Large new bone formation bridging disc space

FIGURE 6 Score of vertebra body changes using clinical computed tomography (CT) over 12 months. A, Before surgical intervention, all specimens had normal vertebral bodies (score of 0). At 3, 6, 9, and 12 months, the Intact group had a lower score than both Injured and FibGen groups. Compared to 0-month baseline, the FibGen group had a larger score at 3, 6, 9, and 12 months, while the Injured group had a higher score at 9 and 12 months. B, The clinical CT scans were scored from 0 to 4 with 0 indicating normal vertebral bodies and 4 indicating vertebral bodies with bone bridging the IVD space. $^{*}P < .05$ compared to Injured and FibGen groups, $^{\#}P < .05$ compared to 0-month baseline

samples.[32] Here, we observed torque range values for Injured and FibGen samples which were beyond the range of similarly aged level matched intact samples,[32] suggesting the high interspecimen variability seen in this model may be due to fibrotic healing or boney changes occurring in vivo. Interestingly, the Wilke group observed decreased range of motion from nucleotomy after 12 weeks in vivo in contrast to increased range of motion seen in vitro, suggesting an in vivo stiffening process, such as the irregular bone formation seen here.[40] Evidence for healing in Injured and FibGen samples are similar to a previous ovine study with a similar sample size with puncture and concentric tear injuries that exhibited significantly reduced bending stiffness after 1 month, followed by an increase in stiffness concurrent with lamellar thickening at 3, 6, 12, and 18 months.[42] The relatively high variance in biomechanical properties and relatively low sample size is a limitation of this study; the required sample size given an effect size of 0.3 and the observed SD (from 4° torque range measurement) is 44 which was cost prohibitive for this long-term in vivo study. Nevertheless, the Injured and FibGen had nearly identical mean values providing little suggestion that a difference would be detected even with an increased sample size. One limitation for this study was there was no fluid bath for these specimens which is known to change the measured response, as

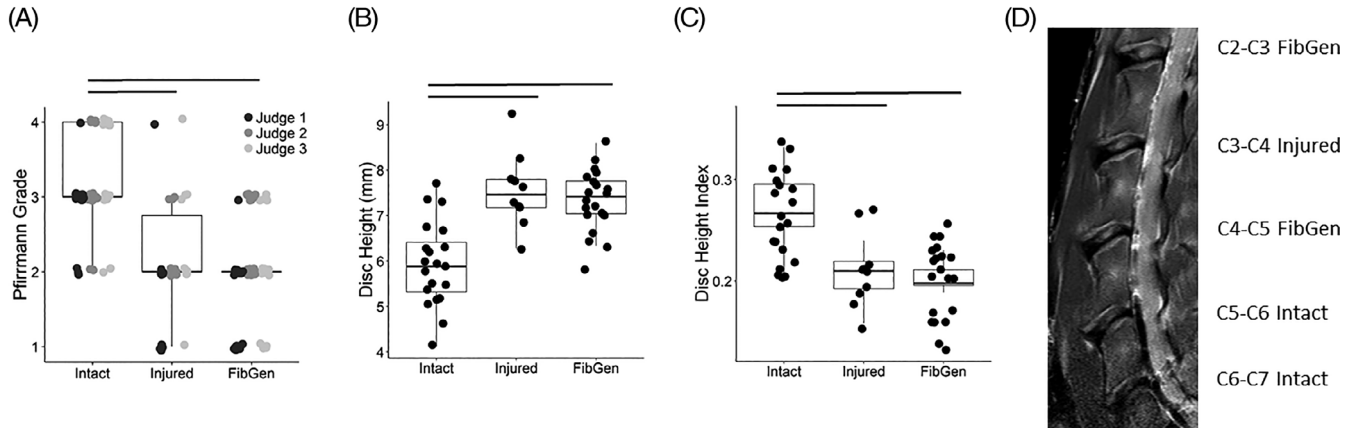

FIGURE 7 IVD height and Pfirrmann grade of MRI after 12 months. A, The Pfirrmann grade of the Intact group was higher than the Injured and FibGen groups, indicating higher degeneration. B, The IVD height was lower in the Intact groups compared to Injured and FibGen groups. C, The disc height index, which is IVD height normalized by inferior vertebral body height, was higher for the Intact group compared to Injured and FibGen. D, Representative MRI of ovine cervical spine after 12 months

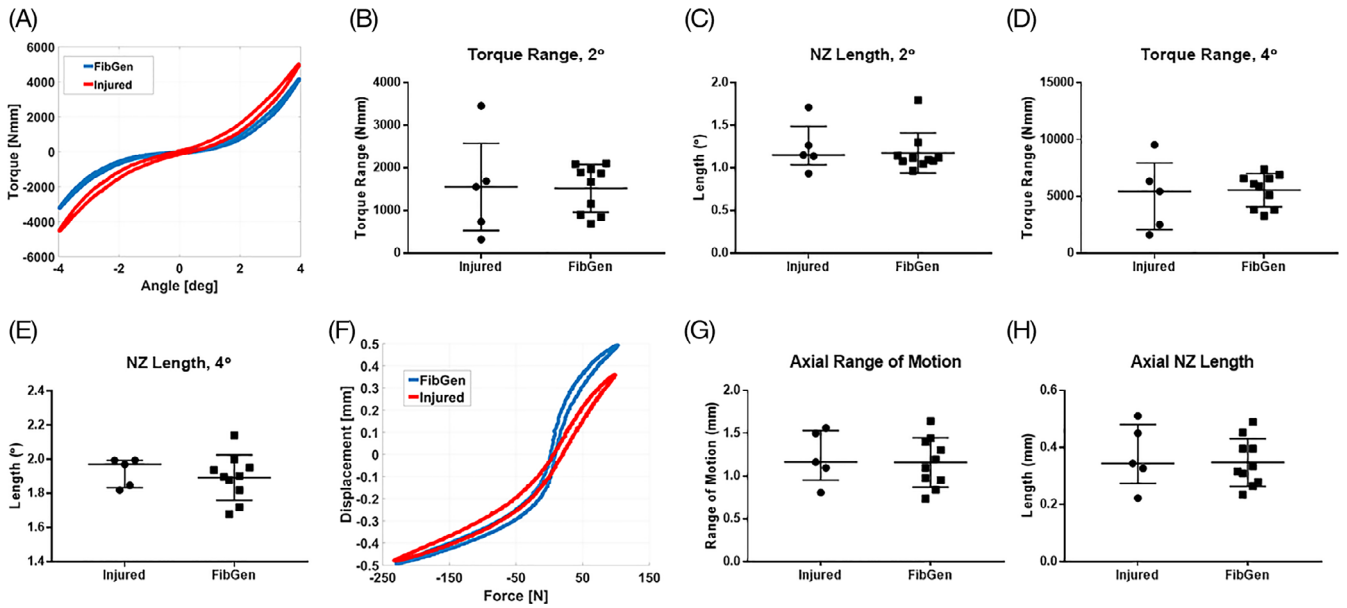

FIGURE 8 Biomechanical response of motion segments after 12 months. A, Representative torque rotation curves from Injured (level C2-C3) and FibGen (level C3-C4) from the same animal. There were no detected differences between Injured and FibGen groups for B, ±2° torque range (P = .59), C, ±2° neutral zone length (p = or D. ±4° torque range (P = .59) axial range of motion (P = .76) was detected between Injured and FibGen samples. D, E, Torque rotation curves from the same specimens. F, No differences in ±4° neutral zone length were detected (P = .87)

decreased water content due to osmotic loading reduces strain energy density and modulus of AF tissue.[42]

Equivalent healing for FibGen and Injured are somewhat similar to prior results for fibrin. Fibrin sealant (Biostat BIOLOGX, Spinal Restorations) showed promise to repair denucleated porcine IVDs after 12 weeks in vivo[43] but then showed equivalency to saline injection in a Phase III clinical trial which was applied to treat single-level discogenic back pain in humans.[44,45] FibGen degrades much more slowly than fibrin alone and we therefore expected FibGen to have greater potential for improved performance for AF repair and biomechanical restoration at 12 months. However, future testing in an injury model with fewer endplate effects will be required to better challenge FibGen and to test this concept.

In the long-term study, we observed irregular vertebral body bone formation starting at 3 months in both injured groups with no difference between FibGen repaired and nonrepaired Injured group. The boney changes were present at 3 months and did not worsen significantly from the third month to the 12th month. This suggests a 3-month timepoint would be appropriate for capturing off-target osteogenic changes with clinical CT which is a noninvasive nondestructive measurement. Potential causes of the vertebral body changes were iatrogenic disruption of the endplate during surgery from the biopsy punch, or remodeling of the endplate in response to degeneration or material implantation. Other ovine models of AF injury showed vertebral body changes including remodeling of the endplate and osteophyte formation following annular injury,[47,48] suggesting additional evidence for heterotopic ossification in ovine in vivo models. Endplate changes were seen in response to scalpel blade incisions suggesting remodeling from AF injury and more severe IVD degeneration.[47,48] Differences in cortical bone structure were also present in an enzyme induced degeneration model,[49] further suggesting IVD health affects vertebral body morphology.

Histological results also demonstrated equivalency between Injured and FibGen groups; however, there was also no evidence for hydrogel related complications. We adopted a scoring scheme which was sensitive to cell treated injured IVDs.[38] Qualitatively, AF structure appeared similar for FibGen and Injured, and there were no semiquantitative differences, suggesting that FibGen adhesive hydrogel was no more effective at restoring the AF structure than the natural healing process. Interestingly, intradiscal blood, blood vessels, and cellular influx were observed which likely resulted from the AF injury. Intradiscal hemosiderin can result from bleeding concurrent to IVD injury and has been observed in the thoracic[50] and lumbar spine.[51] The healthy IVD has minimal vascularization, but increased vascularization is concurrent with degeneration[52] and may result from AF disruption.[53] Future studies in mouse could identify the phenotype and source of cells at the injury site.[53,54]

Interestingly, we observed higher Pfirrmann grade in Intact samples, which typically correlates with higher degeneration.[56] We also observed smaller disc height and larger disc height index for the Intact samples, likely due to naturally reduced disc height but possibly due to adjacent level effects. Previous observations of Merino sheep show less than 0.5 mm difference in average disc height between the cervical levels[56] which is in contrast to the 1 mm difference observed here. Measuring the disc height change longitudinally with higher resolution CT scanning and further normalizing 12 month to 0 month measurements may more accurately represent changes to disc height in each experimental group. As a result, we conclude that intact samples must be controlled for level, and while intact MRI output measurements are presented, the most relevant comparisons are between Injured and FibGen groups which are controlled for level effects.

5 | CONCLUSIONS

This study applied a composite AF repair strategy to a 2-mm diameter biopsy punch injury in an in vivo ovine model to demonstrate that the PTMC scaffold herniated within 1-month while FibGen did not, motivating its further application for long-term repair. At 12 months, Injury and FibGen groups had equivalent fibrotic healing responses with loss of AF fiber continuity, reduction of proteoglycans, formation of intradiscal vessels and similar biomechanical responses. However, AF injury resulted in relatively mild degeneration with high variation due to osteophyte formation and ossification from punch-related endplate damage. Since there was no evidence for hydrogel-related complications in any measurements, we conclude that FibGen may warrant further evaluation, possibly as a delivery vehicle for bioactive therapeutics, for improved healing in a refined AF injury model, perhaps with AF scalpel injury through the nucleus pulposus to minimize potential for endplate damage during the surgical procedure.

ACKNOWLEDGMENTS

This work was funded by the AO Foundation AF Repair Consortium, AO Spine International, National Institute of Arthritis, Musculoskeletal and Skin Disorders of the National Institutes of Health by Grant R01AR057397 and the Whitaker Foundation. The authors thank Drs. Sven Hoppe, Saad Chaudhary, and Andrew Hecht for assistance with MRI analysis, and Nora Goudsouzian, Dieter Wahl, and Ivan Zderic for technical support.

CONFLICT OF INTEREST

DS and MA are editors of JOR Spine and JCI is a named inventor on an issued patent relating to Crosslinked Fibrin Hydrogels for Intervertebral Disc Annulus Fibrosus Repair.

AUTHORS' CONTRIBUTIONS

R.G.L., S.J.F., L.B., D.S., Z.L., A.P., D.W.G., D.E., S.Z., M.A., J.C.I., and S.G. designed the research. L.B., T.S., D.S., and S.Z. performed the surgeries. D.E., A.P., D.W.G., and J.C.I. supplied new materials. R.G.L., U.E., D.N., T.D.T., and T.S. analyzed data. R.G.L., J.C.I., and S.G. wrote the manuscript and all authors revised.

DATA AVAILABILITY STATEMENT

The processed data required to reproduce these findings are available by contacting the authors.

ORCID

Rose G. Long https://orcid.org/0000-0001-9999-9288
Dirk Nehrbass https://orcid.org/0000-0002-4871-5473
Mauro Alini https://orcid.org/0000-0002-0262-1412
James C. Iatridis https://orcid.org/0000-0002-2186-0590
Sibylle Grad https://orcid.org/0000-0001-9552-3653

REFERENCES

1. Livshits G, Popham M, Malkin I, et al. Lumbar disc degeneration and genetic factors are the main risk factors for low back pain in women: the UK Twin Spine Study. *Ann Rheum Dis*. 2011;*70*(10):1740-1745.
2. GBD 2015 DALYs and HALE Collaborators. Global, regional, and national disability-adjusted life-years (DALYs) for 315 diseases and injuries and healthy life expectancy (HALE), 1990-2015: a systematic analysis for the Global Burden of Disease Study 2015. *Lancet*. 2016;*388*(10053):1603-1658.
3. Moore RJ, Vernon-Roberts B, Fraser RD, Osti OL, Schembri M. The origin and fate of herniated lumbar intervertebral disc tissue. *Spine*. 1996;*21*(18):2149-2155.
4. Carragee EJ, Han MY, Suen PW, Kim D. Clinical outcomes after lumbar discectomy for sciatica: the effects of fragment type and anular competence. *J Bone Joint Surg Am*. 2003;*85*(1):102-108.
5. Lim K-Z, Daly CD, Ghosh P, et al. Ovine lumbar intervertebral disc degeneration model utilizing a lateral retroperitoneal drill bit injury. *J Vis Exp*. 2017;*123*:e55753. https://doi.org/10.3791/55753.
6. Melrose J, Burkhardt D, Taylor TKF, et al. Calcification in the ovine intervertebral disc: a model of hydroxyapatite deposition disease. *Eur Spine J*. 2009;*18*(4):479-489.
7. Shu C, Hughes C, Smith SM, et al. The ovine newborn and human foetal intervertebral disc contain perlecan and aggrecan variably substituted with native 7D4 CS sulphation motif: spatiotemporal immunolocalisation and co-distribution with Notch-1 in the human foetal disc. *Glycoconj J*. 2013;*30*(7):717-725.
8. Melrose J, Shu C, Young C, et al. Mechanical destabilization induced by controlled annular incision of the intervertebral disc dysregulates metalloproteinase expression and induces disc degeneration. *Spine*. 2012;*37*(1):18-25.
9. Schollum ML, Appleyard RC, Little CB, Melrose J. A detailed microscopic examination of alterations in normal anular structure induced by mechanical destabilization in an ovine model of disc degeneration. *Spine*. 2010;*35*(22):1965-1973.
10. O'Connell GD, Vresilovic EJ, Elliott DM. Comparison of animals used in disc research to human lumbar disc geometry. *Spine*. 2007;*32*(3):328-333.
11. Maroudas A. Biophysical chemistry of cartilaginous tissues with special reference to solute and fluid transport. *Biorheology*. 1975;*12*(3-4):233-248.
12. Horner HA, Urban JP. 2001 Volvo Award Winner in Basic Science Studies: effect of nutrient supply on the viability of cells from the nucleus pulposus of the intervertebral disc. *Spine*. 2001;*26*(23):2543-2549.
13. Trout JJ, Buckwalter JA, Moore KC, Landas SK. Ultrastructure of the human intervertebral disc. I. Changes in notochordal cells with age. *Tissue Cell*. 1982;*14*(2):359-369.
14. Melrose J, Smith S, Ghosh P. Assessment of the cellular heterogeneity of the ovine intervertebral disc: comparison with synovial fibroblasts and articular chondrocytes. *Eur Spine J*. 2003;*12*(1):57-65.
15. Reitmaier S, Schmidt H, Ihler R, et al. Preliminary investigations on intradiscal pressures during daily activities: an in vivo study using the merino sheep. *PLoS ONE*. 2013;*8*(7):e69610.
16. Wilke HJ, Kettler A, Claes LE. Are sheep spines a valid biomechanical model for human spines? *Spine*. 1997;*22*(20):2365-2374.
17. Bateman AH, Balkovec C, Akens MK, et al. Closure of the annulus fibrosus of the intervertebral disc using a novel suture application device-in vivo porcine and ex vivo biomechanical evaluation. *Spine J*. 2016;*16*(7):889-895.
18. Thomé C, Klassen PD, Bouma GJ, et al. Annular closure in lumbar microdiscectomy for prevention of reherniation: a randomized clinical trial. *Spine J*. 2018;*18*(12):2278-2287.
19. Kienzler JC, Klassen PD, Miller LE, et al. Three-year results from a randomized trial of lumbar discectomy with annulus fibrosus occlusion in patients at high risk for reherniation. *Acta Neurochir (Wien)*. 2019;*161*(7):1389-1396.
20. Wismer N, Grad S, Fortunato G, Ferguson SJ, Alini M, Eglin D. Biodegradable electrospun scaffolds for annulus fibrosus tissue engineering: effect of scaffold structure and composition on annulus fibrosus cells in vitro. *Tissue Eng Part A*. 2014;*20*(3-4):672-682.
21. Martin JT, Milby AH, Chiaro JA, et al. Translation of an engineered nanofibrous disc-like angle-ply structure for intervertebral disc replacement in a small animal model. *Acta Biomater*. 2014;*10*(6):2473-2481.
22. Jeong CG, Francisco AT, Niu Z, Mancino RL, Craig SL, Setton LA. Screening of hyaluronic acid-poly(ethylene glycol) composite hydrogels to support intervertebral disc cell biosynthesis using artificial neural network analysis. *Acta Biomater*. 2014;*10*(8):3421-3430.
23. Long RG, Torre OM, Hom WW, Assael DJ, Iatridis JC. Design requirements for annulus fibrosus repair: review of forces, displacements, and material properties of the intervertebral disk and a summary of candidate hydrogels for repair. *J Biomech Eng*. 2016;*138*(2):021007.
24. Hussain I, Sloan SR, Wipplinger C, et al. Mesenchymal stem cell-seeded high-density collagen gel for annular repair: 6-week results from in vivo sheep models. *Neurosurgery*. 2019;*85*(2):E350-E359.
25. Bowles RD, Setton LA. Biomaterials for intervertebral disc regeneration and repair. *Biomaterials*. 2017;*129*:54-67.
26. Guterl CC, See EY, Blanquer SBG, et al. Challenges and strategies in the repair of ruptured annulus fibrosus. *Eur Cell Mater*. 2013;*25*:1-21.
27. Iatridis JC, Nicoll SB, Michalek AJ, Walter BA, Gupta MS. Role of biomechanics in intervertebral disc degeneration and regenerative therapies: what needs repairing in the disc and what are promising biomaterials for its repair? *Spine J*. 2013;*13*(3):243-262.
28. Schek RM, Michalek AJ, Iatridis JC. Genipin-crosslinked fibrin hydrogels as a potential adhesive to augment intervertebral disc annulus repair. *Eur Cell Mater*. 2011;*21*:373-383.
29. Likhitpanichkul M, Dreischarf M, Illien-Junger S, et al. Fibrin-genipin adhesive hydrogel for annulus fibrosus repair: performance evaluation with large animal organ culture, in situ biomechanics, and in vivo degradation tests. *Eur Cell Mater*. 2014;*28*:25-37. discussion 37.
30. Long RG, Bürki A, Zysset P, et al. Mechanical restoration and failure analyses of a hydrogel and scaffold composite strategy for annulus fibrosus repair. *Acta Biomater*. 2016;*30*:116-125.
31. Pirvu T, Blanquer SBG, Benneker LM, et al. A combined biomaterial and cellular approach for annulus fibrosus rupture repair. *Biomaterials*. 2015;*42*:11-19.
32. Long RG, Zderic I, Gueorguiev B, et al. Effects of level, loading rate, injury and repair on biomechanical response of ovine cervical intervertebral discs. *Ann Biomed Eng*. 2018;*46*(11):1911-1920.
33. Deml MC, Benneker LM, Schmid T, et al. Ventral surgical approach for an intervertebral disc degeneration and regeneration model in sheep cervical spine: anatomic technical description, strengths and limitations. *Vet Comp Orthop Traumatol*. 2019;*32*(5):389-393.
34. Schindelin J, Arganda-Carreras I, Frise E, et al. Fiji: an open-source platform for biological-image analysis. *Nat Methods*. 2012;*9*(7):676-682.
35. Masuda K, Aota Y, Muehleman C, et al. A novel rabbit model of mild, reproducible disc degeneration by an anulus needle puncture: correlation between the degree of disc injury and radiological and histological appearances of disc degeneration. *Spine*. 2005;*30*(1):5-14.

36. Pearcy MJ, Tibrewal SB. Axial rotation and lateral bending in the normal lumbar spine measured by three-dimensional radiography. *Spine*. 1984;*9*(6):582-587.
37. Smit TH, van Tunen MS, van der Veen AJ, Kingma I, van Dieën JH. Quantifying intervertebral disc mechanics: a new definition of the neutral zone. *BMC Musculoskelet Disord*. 2011;*12*:38.
38. Shu CC, Smith MM, Smith SM, Dart AJ, Little CB, Melrose J. A histopathological scheme for the quantitative scoring of intervertebral disc degeneration and the therapeutic utility of adult mesenchymal stem cells for intervertebral disc regeneration. *Int J Mol Sci*. 2017;*18*(5):1049. https://doi.org/10.3390/ijms18051049
39. The R Foundation for Statistical Computing RCT. *R: A Language and Environment for Statistical Computing*. Vienna, Austria: The R Foundation for Statistical Computing; 2018.
40. Shrout PE, Fleiss JL. Intraclass correlations: uses in assessing rater reliability. *Psychol Bull*. 1979;*86*(2):420-428.
41. Reitmaier S, Volkheimer D, Berger-Roscher N, Wilke H-J, Ignatius A. Increase or decrease in stability after nucleotomy? Conflicting in vitro and in vivo results in the sheep model. *J R Soc Interface*. 2014;*11*(100):20140650.
42. Fazzalari NL, Costi JJ, Hearn TC, et al. Mechanical and pathologic consequences of induced concentric anular tears in an ovine model. *Spine*. 2001;*26*(23):2575-2581.
43. Werbner B, Spack K, O'Connell GD. Bovine annulus fibrosus hydration affects rate-dependent failure mechanics in tension. *J Biomech*. 2019;*89*:34-39.
44. Buser Z, Kuelling F, Liu J, et al. Biological and biomechanical effects of fibrin injection into porcine intervertebral discs. *Spine*. 2011;*36*(18):E1201-E1209.
45. Yin W, Pauza K, Olan WJ, Doerzbacher JF, Thorne KJ. Intradiscal injection of fibrin sealant for the treatment of symptomatic lumbar internal disc disruption: results of a prospective multicenter pilot study with 24-month follow-up. *Pain Med*. 2014;*15*(1):16-31.
46. National Library of Medicine. ClinicalTrials.gov [Internet]. Identifier NCT01011816, Treatment of Symptomatic Lumbar Internal Disc Disruption (IDD) With the Biostat® System; 2014. https://clinicaltrials.gov/ct2/show/NCT01011816. Cited January 17, 2019.
47. Melrose J, Smith SM, Little CB, Moore RJ, Vernon-Roberts B, Fraser RD. Recent advances in annular pathobiology provide insights into rim-lesion mediated intervertebral disc degeneration and potential new approaches to annular repair strategies. *Eur Spine J*. 2008;*17*(9):1131-1148.
48. Moore RJ, Vernon-Roberts B, Osti OL, Fraser RD. Remodeling of vertebral bone after outer anular injury in sheep. *Spine*. 1996;*21*(8):936-940.
49. Gullbrand SE, Malhotra NR, Schaer TP, et al. A large animal model that recapitulates the spectrum of human intervertebral disc degeneration. *Osteoarthr Cartil*. 2017;*25*(1):146-156.
50. Miyakoshi N, Hongo M, Kasukawa Y, Ando S, Shimada Y. Thoracic disk herniation with hematoma—case report. *Neurol Med Chir (Tokyo)*. 2008;*48*(9):414-417.
51. Watanabe N, Ogura T, Kimori K, Hase H, Hirasawa Y. Epidural hematoma of the lumbar spine, simulating extruded lumbar disk herniation: clinical, discographic, and enhanced magnetic resonance imaging features. A case report. *Spine*. 1997;*22*(1):105-109.
52. Kauppila LI. Ingrowth of blood vessels in disc degeneration. Angiographic and histological studies of cadaveric spines. *J Bone Joint Surg Am*. 1995;*77*(1):26-31.
53. Stefanakis M, Al-Abbasi M, Harding I, et al. Annulus fissures are mechanically and chemically conducive to the ingrowth of nerves and blood vessels. *Spine*. 2012;*37*(22):1883-1891.
54. Torre OM, Mroz V, Bartelstein MK, Huang AH, Iatridis JC. Annulus fibrosus cell phenotypes in homeostasis and injury: implications for regenerative strategies. *Ann N Y Acad Sci*. 2019;*1442*(1):61-78.
55. Habtemariam A, Virri J, Grönblad M, Holm S, Kaigle A, Karaharju E. Inflammatory cells in full-thickness anulus injury in pigs. An experimental disc herniation animal model. *Spine*. 1998;*23*(5):524-529.
56. Pfirrmann CW, Metzdorf A, Zanetti M, Hodler J, Boos N. Magnetic resonance classification of lumbar intervertebral disc degeneration. *Spine*. 2001;*26*(17):1873-1878.
57. Wilke HJ, Kettler A, Wenger KH, Claes LE. Anatomy of the sheep spine and its comparison to the human spine. *Anat Rec*. 1997;*247*(4):542-555.

SUPPORTING INFORMATION

Additional supporting information may be found online in the Supporting Information section at the end of this article.

How to cite this article: Long RG, Ferguson SJ, Benneker LM, et al. Morphological and biomechanical effects of annulus fibrosus injury and repair in an ovine cervical model. *JOR Spine*. 2020;3:e1074. https://doi.org/10.1002/jsp2.1074